An Accurate Modeling and Suppression Method for Current Imbalance in Dual-Receiver WPT Systems for Low-voltage and High-current Applications

Yong Li, *Senior Member*, *IEEE*, Junwen Chen, Yeran Liu, *Member*, *IEEE*, Xing Zhao, *Member*, *IEEE*, Minfan Fu, *Senior Member*, *IEEE*, Zhengyou He, *Senior Member*, *IEEE*

***Abstract*—Wireless power transfer (WPT) technology is a convenient charging method for AGVs without manual operation. To satisfy the low voltage and high current requirement for charging AGVs, the dual-receiver WPT system is used to improve the current capacity and to decrease the current stress in coils and devices. However, the dual-receiver system suffers from current imbalance or even current clamping issues when the coupler misalignment occurs with different mutual inductance on each receiver channel. The current imbalance defeats the original purpose of the design and causes receiver overload and device overstress. Therefore, this paper presents an accurate model to describe the dual receiver currents under coupler misalignment. The key factors and reason of the current imbalance are studied accordingly and then guide the design of the coupler and the circuit of the dual-receiver system. Moreover, according to the practical demand, a comprehensive control strategy is proposed to achieve current balance and constant voltage output simultaneously. Finally, an experimental prototype of 48V/30A is built to validate the proposed method. The experimental results show that with the control strategy, the current difference can be decreased from 29.31A to 0.26A under various misalignment conditions, while the efficiency increases by 1.8%.**

***Index Terms*—Wireless power transfer (WPT), dual-receiver, current balance, hardware PQ decomposition.**

I. Introduction

Wireless power transfer (WPT) systems have been widely used in various fields, such as electric vehicles (EVs), automated guided vehicles (AGVs), unmanned aerial vehicles (UAVs) [1]-[4], due to their safety, reliability, and convenience. In the applications of AGVs, the WPT systems can charge the battery of the AGV wirelessly and avoid the risk of spark and mechanical fault of the chargers, which is suitable for the industrial field. In order to achieve fast charging of AGVs, the charging power is relatively large. However, because the voltage of the batteries in AGVs is commonly 24V or 48V, the receiver current of the WPT charging system is at least tens of amperes, which is also called the low-voltage and high-current system [5]-[7].

For the low-voltage and high-current WPT systems, the main challenges are the high rating requirement of the switches in the rectifier, higher coil losses, and lower system efficiency. Besides, the volume of the heat sink in a high-current system is also larger. In general, the high-current WPT system requires higher cost and volume of components, which is not suitable for massive lightweight AGVs.

In order to decrease the current stress, two kinds of methods have been proposed including:1) current-doubler rectifier, and 2) multi-receiver. In the current-doubler rectifier, the DC output current is twice larger than the receiver coil current, thus reducing the AC current stress of the coil and rectifier and resulting in lower losses and higher efficiency [8], [9]. However, the current doubler rectifier has a significant increase in weight because two independent inductors are used for storing energy. Besides, the output characteristics of the current doubler rectifier are not suitable for the simplest series-series (S-S) compensated WPT systems. In order to solve this problem, an inverse coupled current doubler is proposed to be compatible with the S-S WPT system in [10] and [11]. However, the leakage inductance of the inverse coupled current doubler causes a high voltage ringing of the diode and reduces the stability of the system.

Alternatively, the multi-receiver system is another approach to achieve high output current, which has been used for various purposes, such as offset immunity, multi-output, and power capacity enhancement[12]-[18]. For the high-current system, the parallel multi-receiver structure has the following advantages. Firstly, advanced but expensive components for the single-receiver system can be replaced by common and cheaper components. Secondly, the cost and volume of heat dissipation can be decreased. Thirdly, it is easy to combine several receiver modules flexibly for specific current/power requirements.

However, the current imbalance is a common and critical issue for the multi-receiver system, which will lead to the current increase of one receiver significantly. For example, to obtain a total output power of 2kW, the capacity of each receiver will ideally be designed to be 1kW. Considering a margin of 50%, each receiver can only provide a maximum power of 1.5kW. If the current imbalance or current clamping occurs, it means that one receiver has to provide 1.8kW power or even the whole 2kW power, therefore causing significant temperature rising or even component breakdown. On the other hand, because the series resonant topology is used on the receiver side, when the current imbalance occurs, the voltage of the resonant capacitor also increases which can lead to the

This work was supported in part by National Natural Science Foundation of China under Grant 52377016, in part by the Sichuan Science and Technology Program under Grant 2023NSFSC0001, in part by National Natural Science Foundation of China under Grant 52107209. (Corresponding author: Yeran Liu)

Yong Li, Junwen Chen, Yeran Liu, Xing Zhao, Minfan Fu, and Zhengyou He are with the School of Electrical Engineering, Southwest Jiaotong University, Chengdu 610031, China (e-mail: leeo1864@163.com; chenjwswjtu@163.com; yeranliu@my.swjtu.edu.cn; hezy@swjtu.edu.cn).

X. Zhao is with the School of Physics, Engineering and Technology with University of York, York YO10 5DD, U.K. (e-mail: xing.zhao@york.ac.uk.)

Minfan Fu is with the School of Information Science and Technology, ShanghaiTech University, Shanghai 201210, China (e-mail: fumf@shanghaitech.edu.cn).

overvoltage breakdown of the resonant capacitor. If the current imbalance or current clamping is not addressed, the dual-receiver WPT system will not be able to be applied in practice.

In order to address the current imbalance issue of dual-receiver systems, several methods are proposed to model the imbalanced receiver circuit and to mitigate the imbalanced currents [19]-[21]. The most typical current clamping phenomenon is analyzed in [19] by modeling the clamped rectifier as a totally turned-off device, and a method that utilizes the cross-coupling and detuned receivers is proposed to avoid the current clamping. Because only the current clamping condition is modeled, the current imbalance is decreased by 55.8% but still exists. To further analyze the current imbalance, the rectifier and the load of each receiver are modeled as AC resistors with equal values in [20]- [21]. This method is applicable only when the output current of each receiver is the same and shows the trend of current change inaccurately. In general, an accurate model for analyzing the current imbalance of multi-receiver WPT systems has not been reported yet.

Moreover, although it is roughly known that the mutual inductance difference is the main reason for the current imbalance in multi-receiver systems, the detailed influence factors and the boundary that causes current clamping are not clear yet. The variation of the current imbalance with various mutual inductance conditions is also unknown, which makes it difficult to design and control the multi-receiver systems for the purpose of totally mitigating the current imbalance.

Therefore, in this paper, an accurate model to describe the current imbalance of a dual-receiver WPT is derived by equating two receiver circuits with two DC voltages in series with equivalent resistors. The key factors that cause the current imbalance, including the mutual inductance ratio and the equivalent DC voltages, are investigated in detail. According to the influence factors derived from the current imbalance model, both the system and the control strategy are well-designed to mitigate the current imbalance. In order to suppress the mutual inductance difference, a coupler with a double-D and quadruple-D pad (DD-QDP) structure is designed. Meanwhile, a circuit with active rectifiers as well as a comprehensive control strategy is proposed to adjust the equivalent DC voltages of the two receivers. Finally, a 48V/30A experimental prototype was built to validate this method, in which the current difference is decreased from 29.31A to 0.26A, while the efficiency is improved by 1.8%.

The accurate model to describe the current imbalance of the dual receiver system is given in Section II. Based on the key influence factors of the current imbalance, the coil structure and the circuit with active rectifiers are designed in Section III, and the corresponding control strategy to achieve accurate current balance is proposed in Section IV. Finally, the experiments are carried out in Section V to validate the proposed method.

II. Current Imbalance Model of Dual-Receiver WPT Systems With Two Passive Rectifiers

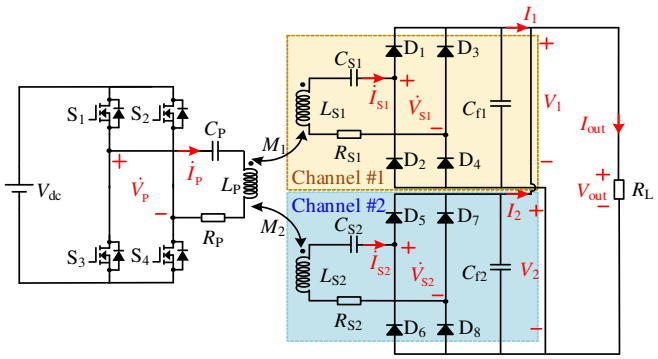

Fig. 1. Circuit scheme of the dual-receiver WPT system on the secondary side.

The dual-receiver WPT system with two passive rectifiers is shown in Fig. 1. In this system, the receivers are connected in parallel to the load. V_{dc} is the DC input voltage, V_{out} and I_{out} are the DC output voltage and current, respectively, and R_L is the resistive load of the system. M_1 and M_2 are the mutual inductances between the primary and secondary coils, respectively. The cross-coupling between the two secondary coils is neglected. L_P, L_{S1}, and L_{S2} are the self-inductances, and R_P, R_{S1}, and R_{S2} are the equivalent series resistances (ESRs) of the coils. C_P, C_{S1}, and C_{S2} denote the series-resonant capacitors. To compensate the self-inductance of the coils on the primary and secondary sides, C_P, C_{S1}, and C_{S2} should satisfy:

$$\omega = \frac{1}{\sqrt{L_P C_P}} = \frac{1}{\sqrt{L_{S1} C_{S1}}} = \frac{1}{\sqrt{L_{S2} C_{S2}}} \tag{1}$$

where $\omega = 2\pi f$ denotes the system angular frequency, and f is the operating frequency. In this paper, the fundamental harmonic approximation (FHA) method is used to analyze the circuit.

A. Traditional Model

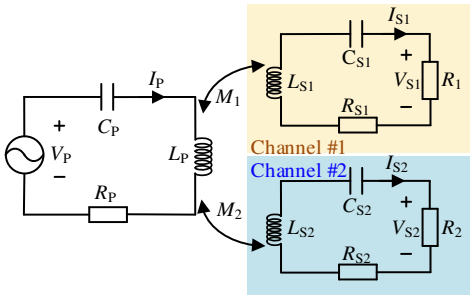

Fig. 2 Phase model of the dual-receiver WPT system

Fig. 2 shows the traditional phasor model of the dual-receiver system, in which two equivalent AC resistors are used to model the paralleled rectifier and the actual load. According to Kirchhoff's voltage law (KVL), the phasor model can be expressed as:

$$\begin{cases} \dot{V}_P = \dot{I}_P\left(R_P + j\omega L_P + \dfrac{1}{j\omega C_p}\right) - \mathrm{j}\omega M_1 \dot{I}_{S1} - \mathrm{j}\omega M_2 \dot{I}_{S2} \\ \mathrm{j}\omega M_1 \dot{I}_P = \dot{I}_{S1}\left(R_{S1} + R_1 + j\omega L_{S1} + \dfrac{1}{j\omega C_{S1}}\right) \\ \mathrm{j}\omega M_2 \dot{I}_P = \dot{I}_{S2}\left(R_{S2} + R_2 + j\omega L_{S2} + \dfrac{1}{j\omega C_{S2}}\right) \end{cases} \tag{2}$$

The relationship between the load resistor R_L and the equivalent ac load resistors R_1 and R_2 in the two receiver circuits is expressed as:

$$\frac{1}{R_1}+\frac{1}{R_2}=\frac{\pi^2}{8R_L} \tag{3}$$

However, in order to solve R_1 and R_2 respectively, the power distribution or the mutual inductance between the two receivers needs to be known first. In the previous literature [19], it is assumed that M_1=M_2. Then R_1 and R_2 are solved as:

$$R_1=R_2=\frac{16}{\pi^2}R_L \tag{4}$$

And the receiver coil currents are expressed as:

$$\begin{cases}\dot{I}_{S1}=\dfrac{j\omega M_1}{R_{S1}+16R_L/\pi^2}\dot{I}_P\\ \dot{I}_{S2}=\dfrac{j\omega M_2}{R_{S2}+16R_L/\pi^2}\dot{I}_P\end{cases} \tag{5}$$

According to (5), it can be easily obtained that the output current ratio $\dot{I}_{S1}/\dot{I}_{S2}$ is proportional to the mutual inductance ratio M_1/M_2. But this is inconsistent with the actual phenomenon under various conditions except for M_1≈M_2. Thus, it can't explain the current imbalance and current clamping issues, which brings complexity and confusion in designing and controlling the dual-receiver system.

B. *Proposed Model*

In order to represent the characters of the dual-receiver system more clearly, the current relationship of the two receivers is analyzed from the view of DC analysis. Ideally, the resonance frequency in each coil loop and the switching frequency should be the same in a WPT system in order to decrease the reactive power. Indeed, due to the component error, the difference among these frequencies may exist. But, the resonant frequency difference between the two resonant tanks is quite small which has little effect on current distribution. So, the frequency difference can be ignored here and the receiving circuits are in resonant condition. It can be easily found that $\dot{V}_{Si}$ is in phase with $\dot{I}_{Si}$ and 90 degrees ahead of $\dot{I}_P$. Therefore, (2) can be simplified by the RMS value as:

$$\begin{cases}V_P=I_PR_P-\omega M_1I_{S1}-\omega M_2I_{S2}\\ V_{Si}=\omega M_iI_P-I_{Si}R_{Si}\quad (i=1,2)\end{cases} \tag{6}$$

Based on (6), the DC output voltage of each rectifier can be obtained as:

$$V_i=\underbrace{\lambda_i(\omega M_iI_P-2V_f)}_{Veqi}-\underbrace{\lambda_i^2R_{Si}I_i}_{Reqi}\quad (i=1,2) \tag{7}$$

where V_f is the forward voltage drop of diodes, and $\lambda_i=\pi/(2\sqrt{2})$ is the voltage gain of the passive rectifier from the AC side to the DC side.

According to (7), a single receiver channel can be equivalent to a voltage source V_{eqi} and a series equivalent resistance R_{eqi} on the DC side as shown in Fig. 3 (a). Then, the DC equivalent circuit of the dual-receiver in parallel is illustrated in Fig. 3 (b). The equivalent voltage and internal resistance are expressed as:

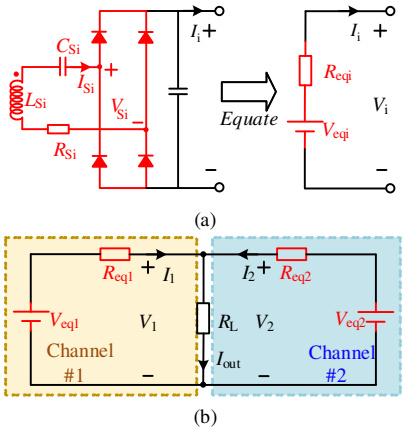

Fig. 3. (a)Equivalent circuit model of a single receiver; (b) Equivalent circuit model of dual-receiver in parallel.

$$\begin{cases}V_{eqi}=\dfrac{\pi}{2\sqrt{2}}(\omega M_iI_P-2V_f)\\ R_{eqi}=\dfrac{\pi^2}{8}R_{Si}\end{cases}\quad i=1,2 \tag{8}$$

By using KVL, the equations of the equivalent DC circuit in Fig. 3 (b) can be derived as:

$$\begin{bmatrix}R_{eq1}+R_L & R_L\\ R_L & R_{eq2}+R_L\end{bmatrix}\cdot\begin{bmatrix}I_1\\ I_2\end{bmatrix}=\begin{bmatrix}V_{eq1}\\ V_{eq2}\end{bmatrix} \tag{9}$$

$$I_{Si}=\frac{\pi}{2\sqrt{2}}I_i \tag{10}$$

The relationship between the DC output current and the AC coil current is shown in (10). By substituting (10) into (9), the two-channel receiver coil currents I_{S1} and I_{S2} can be solved as:

$$\begin{cases}I_{S1}=A_{D1}+B_{D1}\\ I_{S2}=A_{D2}+B_{D2}\\ A_{D1}=\dfrac{\omega R_LI_P(M_1-M_2)}{R_L(R_{S1}+R_{S2})+\dfrac{\pi^2}{8}R_{S1}R_{S2}}\\ A_{D2}=\dfrac{\omega R_LI_P(M_2-M_1)}{R_L(R_{S1}+R_{S2})+\dfrac{\pi^2}{8}R_{S1}R_{S2}}\\ B_{D1}=\dfrac{R_{S2}\cdot(\omega M_1I_P-2V_f)}{\dfrac{8}{\pi^2}R_L(R_{S1}+R_{S2})+R_{S1}R_{S2}}\\ B_{D2}=\dfrac{R_{S1}\cdot(\omega M_2I_P-2V_f)}{\dfrac{8}{\pi^2}R_L(R_{S1}+R_{S2})+R_{S1}R_{S2}}\end{cases} \tag{11}$$

In (11), A_{D1} and A_{D2} have the opposite signs, and B_{D1} and B_{D2} have the same signs. When the diode voltage drop is neglected, B_{D1} and B_{D2} are the same as the result derived from the traditional phasor model. However, additional components A_{D1} and A_{D2} are new terms obtained from the DC analysis, which explains the reason for the current imbalance. For example, when M_1 is greater than M_2, A_{D1} is positive in I_{S1}, but A_{D2} is negative in I_{S2}, resulting in an increase in I_{S1} and a decrease in I_{S2}. The denominator of A_{D1} and A_{D2} contains the ESR of coils (R_{S1}, R_{S2}), which are relatively small components. Therefore, even a small deviation of the mutual inductance will cause a large variation of A_{D1} and A_{D2}. Then, a large current will be generated

in one receiver, leading to current imbalance or current clamping.

TABLE I KEY PARAMETERS FOR THEORETICAL ANALYSIS

Symbol	Quantity	Value
R_L	Equivalent load resistance of the battery packs	1.6 Ω
R_{S1}/R_{S2}	ESR of L_{S1}/L_{S2}	0.1Ω

To validate the accuracy of the proposed model, the two receivers' coil currents that are obtained from the proposed model, the traditional phasor model, and the simulation are compared in Fig. 4 under the condition where M_1 is fixed at 17μH and M_2 varies from 16μH to 18μH. The results from the proposed model are in agreement with the results from the simulation. But the traditional phasor model has significant errors when $M_1 \neq M_2$. Therefore, the proposed model can explain the receiver current more accurately.

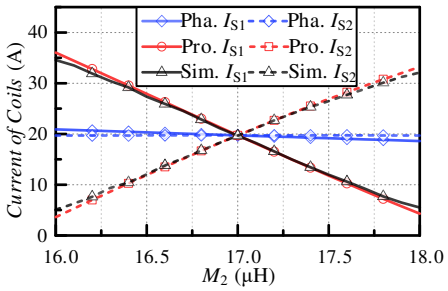

Fig. 4 The result value of coil currents in the phasor model, proposed model, and simulation.

To further analyze the effect of system parameters on the current imbalance concisely, the difference between M_1 and M_2 is described by:

$$M_k = \frac{M_1}{M_2} \tag{12}$$

According to (11) and (12), the ratio of I_{S1} and I_{S2} can be expressed as

$$I_{Sk} = \frac{I_{S1}}{I_{S2}} = \frac{R_L(M_k - 1) + \lambda_2^2 R_{S2} M_k}{R_L(1 - M_k) + \lambda_1^2 R_{S1}} \tag{13}$$

With the parameters listed in TABLE I, the ratio of the two currents I_{Sk} is plotted with R_L varying from 1.6 Ω to 4.8 Ω and R_s varying from 0.1 Ω to 0.2 Ω. In Fig. 5, the current is balanced when M_k is 1. As the value of M_k deviates from 1 slightly, I_k begins to increase even tens or hundreds of times larger. According to the variation of I_{Sk}, it can be concluded that the current imbalance is mainly caused by M_k and can be diminished by larger R_{eq}.

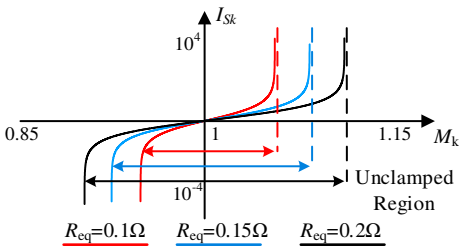

Fig. 5 The operation region of the system

With the increase of the difference between M_1 and M_2, one receiver current will be clamped to zero due to the diode rectifier. According to (13), the current unclamped region of M_k can be derived as:

$$\frac{R_L}{R_L + \lambda_2^2 R_{S2}} \le M_k \le \frac{R_L + \lambda_1^2 R_{S1}}{R_L} \tag{14}$$

When M_k is out of the range expressed in (14), one receiver will be clamped, while another receiver will suffer the load current I_{out} solely. As a result, the current clamping occurs and the components may be damaged. Therefore, the current clamp phenomenon should be avoided when designing the system.

In summary, according to (8), the mutual inductance difference leads to the difference between V_{eq1} and V_{eq2}, and then the current imbalance becomes significant as shown in Fig. 5. As a result, local overheating or even component damage may occur. If the V_{eq} can be adjusted, the current imbalance problem can be addressed.

III. Proposed Dual-Receiver WPT System

According to the analysis in the previous section, it can be found that the key factors to generate the current imbalance are the mutual inductance ratio M_k and the equivalent resistance R_{eq}. Therefore, this section will design the coupler and the circuit of the dual-receiver system considering the two important factors to suppress the current imbalance.

A. Coil design

According to (13), in order to keep the currents of the two receiving coils identical, M_k should be close to 1 as much as possible. Furthermore, for the coil structure used in the AGV scenario, the change of two mutual inductances M_1 and M_2 under both X-axis and Y-axis misalignment should be the same, which means $M_k \approx 1$.

Currently, the common dual receiver coil structure includes bipolar pad (BP) [22] and [23], double-D quadrature (DDQ) [24]. For the DDQ coil structure, it is difficult to realize the same coupling coefficient due to the asymmetric structure. For the BP coil structure despite having a symmetrical coil structure, the coupling coefficient varies asynchronously under X-axis misalignment. Therefore, these two coil structures are not available to address the current imbalance problems.

To satisfy the requirements, a double-D (DD) coil is used as the transmitter, while a quadruple-D pad (QDP) [25] is used as the receiver, as shown in Fig. 6. Ferrite cores are placed on both the transmitter and receivers to improve the coupling ability. For the QDP, the direction of the adjacent coil current is set to be opposite to decouple the two coils. To further illustrate the decoupling characteristics, the magnetic flux induced by the QDP is plotted specifically in Fig. 7. Since the magnetic flux induced by L_{S1} (L_{S2}) is symmetrical in space, the amount of the magnetic flux flowing into L_{S2} (L_{S1}) equals to that flowing out of it. Therefore, the magnetic flux generated by every receiver is zero, and the mutual inductance between them can be regarded as zero.

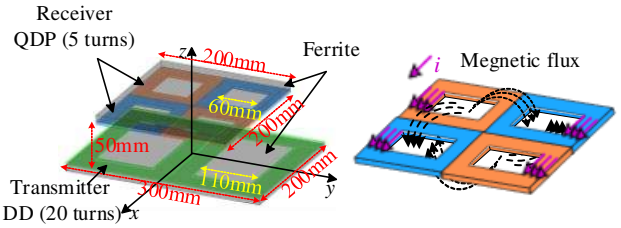

Fig. 6. Structure of the proposed DD-QDP coupler.

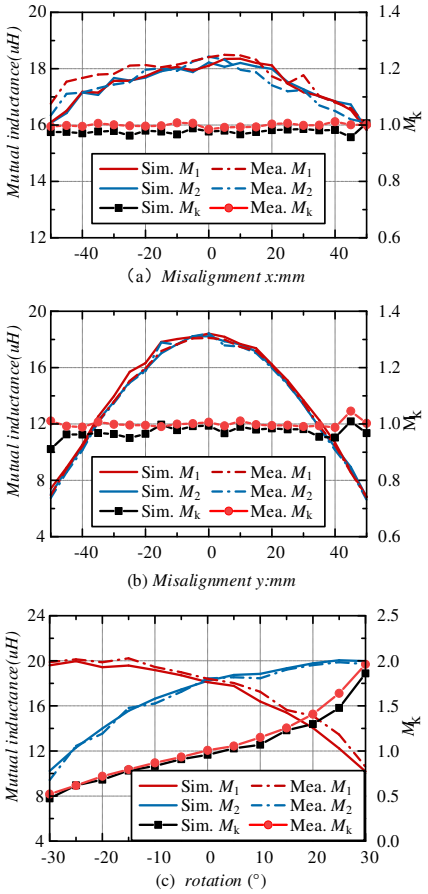

Fig. 7. Variations of mutual inductances under misalignment in (a) *x*-axis, (b) *y*-axis, (c)*rotation*.

The finite element simulation and the experimental measurement are used to validate the variation of the mutual inductance between the transmitter and receiver under misalignment conditions as shown in Fig. 7. In Fig. 7 (a) and (b), it is obvious that the variation trends of M_1 and M_2 are nearly the same, which indicates that the value of M_k is approximately equal to 1. Therefore, the current imbalance will be relieved when the x-axis or y-axis misalignment occurs. However, when the coupler is rotated, as shown in Fig. 7 (c), it will cause a large mutual inductance difference. The value of M_k can be up to 2 and the problem of current imbalance or even current clamping will happen. In order to overcome this problem, an average current control method that adjusts V_{eqi} to suppress the deviation of M_k will be proposed in the next section.

B. *Circuit design*

When the current imbalance is generated by mutual inductance errors, coil rotation, or other problems, active current control is required. This receiver circuit should be capable of modifying the equivalent voltage V_{eq} and increasing the equivalent resistance R_{eq} to suppress the influence of varied M_k. The common approaches include the use of DC-DC modules or active rectifiers. When using DC-DC, it increases the size and weight of the receiver due to the extra inductors and devices. On the contrary, replacing the passive rectifier with an active rectifier has less impact on the overall size which is beneficial for AGVs. Therefore, two active rectifier bridges are adopted to achieve the current balance in the dual-receiver WPT system as shown in Fig. 8.

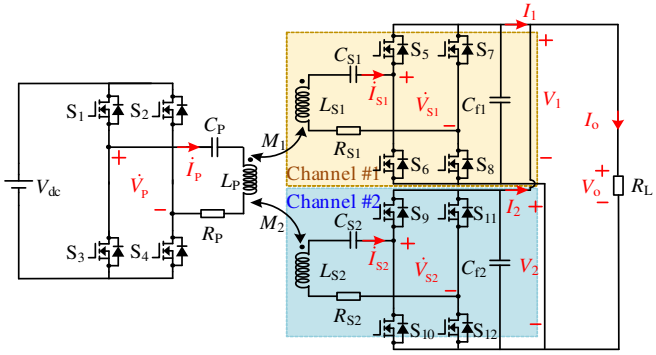

Fig. 8. Proposed circuit scheme of the dual-receiver WPT system

Fig. 9 shows the operation waveforms of the two active rectifiers. α_1 and α_2 are the pulse-width of the dual active receivers, and γ is the angle between the primary side and secondary side. φ_{inv}, φ_{rec1}, and φ_{rec2} are the phase angles between the voltage and current of the inverter and two rectifiers respectively. It should be noted that the angle γ would be generated by ZVS or the detuned system. It is considered here to increase the adaptability of this model.

The analysis method of the active rectifier bridge is similar to that of the passive rectifier bridge. But the expressions of the equivalent parameters V_{eq} and R_{eq} are changed to [30]:

$$\begin{cases} V_{eqi} = \dfrac{\pi}{2\sqrt{2}} \csc\dfrac{\alpha_i}{2}\omega M_i I_P \\ R_{eqi} = \dfrac{\pi^2}{8}\csc^2\dfrac{\alpha_i}{2}\csc^2\dfrac{\gamma}{2}\left(R_{Si} + 2R_{DS(on)}\right) \end{cases} \tag{15}$$

where the $R_{DS(on)}$ represents the conductive resistance of the MOSFET.

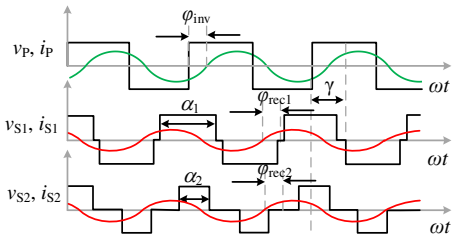

Fig. 9. Waveforms of primary and secondary voltage and current under phase shift control.

In (15), it can be seen that the pulse-width α_i can change the equivalent voltage V_{eqi} and equivalent resistance R_{eqi}, while γ affects the equivalent resistance R_{eqi}. In addition, compared with a nearly constant voltage drop of the diode, the resistive voltage drop of the MOSFET can increase the R_{eq}, contributing to suppressing the current imbalance.

With the control of the active rectifiers, the current ratio of the two receivers can be expressed as:

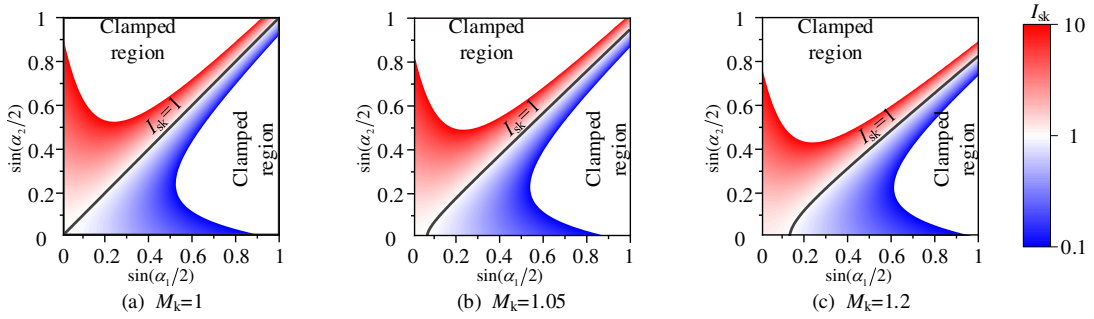

Fig. 10. I_{S1}/I_{S2} as a function of $\sin(\alpha_1/2)$ and $\sin(\alpha_2/2)$ when R_L=1.6 Ω, (a) with M_k=1.0; (b) with M_k =1.05, (c) with M_k =1.2.

$$I_{Sk}=\frac{I_{S1}}{I_{S2}}=\frac{\sin\frac{\alpha_2}{2}\sin^2(\frac{\gamma}{2})R_L\left(k\sin\frac{\alpha_2}{2}-\sin\frac{\alpha_1}{2}\right)+\frac{\pi^2}{8}M_k\left(R_{S2}+2R_{mos}\right)}{\sin\frac{\alpha_1}{2}\sin^2(\frac{\gamma}{2})R_L\left(\sin\frac{\alpha_1}{2}-k\sin\frac{\alpha_2}{2}\right)+\frac{\pi^2}{8}\left(R_{S1}+2R_{mos}\right)} \tag{16}$$

According to (16), I_{S1}/I_{S2} as a function of $\sin(\alpha_1/2)$ and $\sin(\alpha_2/2)$ are plotted in Fig. 10 when R_L=1.6 Ω and M_k varies from 1.0 to 1.2. The black lines mean the relationship between α_1 and α_2 when I_{Sk}=1. Thus, if the mutual inductance ratio M_k changes from 1 to 1.2, the balanced current of the two receivers can be achieved by adjusting α_1 and α_2 properly. When the AC currents are identical, the ratio of the DC currents I_k can be obtained as:

$$I_k=\frac{I_1}{I_2}=\frac{\sin(\alpha_1/2)}{\sin(\alpha_2/2)} \tag{17}$$

Although I_k is related to α_1 and α_2, the difference between α_1 and α_2 is not large when I_{Sk}=1 as shown in Fig.10. Thus, the difference of the DC currents of the two rectifiers are not significant. Besides, the DC side is connected in parallel with conductors whose resistances are very small compared to the coil resistances. Therefore, the influence of the DC current imbalance is small.

Meanwhile, the output voltage with respect to α_1 and α_2 is expressed as:

$$V_o=\frac{2\sqrt{2}}{\pi}\sin(\frac{\alpha_1}{2})\sin(\frac{\gamma}{2})I_{S1}R_L+\frac{2\sqrt{2}}{\pi}\sin(\frac{\alpha_2}{2})\sin(\frac{\gamma}{2})I_{S2}R_L \tag{18}$$

According to (18), there are many combinations of (α_1, α_2) to achieve fixed output voltage. Therefore, the optimal (α_1, α_2) for constant voltage output and balanced currents can be obtained by solving the two equations:

$$\begin{cases}\left.\dfrac{I_{S1}}{I_{S2}}=1\right|_{(\alpha_1,\alpha_2)}\\ \left.V_o=V_o^*\right|_{(\alpha_1,\alpha_2)}\end{cases} \tag{19}$$

IV. Control Strategy

According to (19), the current balance and constant output voltage/current can be achieved by controlling α_1, and α_2. In this section, a detailed control strategy will be given, considering the synchronization and ZVS condition of the active rectifier to increase the feasibility and integrity of the system as much as possible.

A. *Synchronous control*

In the proposed system, two independent digital signal processors (DSP) are used to generate the drive signals to control the on-off state of the MOSFETs on the primary side and secondary side, respectively. Therefore, the two PWM signals need to be synchronized to ensure the stability of the system. The hardware PQ decomposition method is utilized to achieve synchronization, in which the instant active and reactive power of the active rectifier is measured [26]-[28]. By controlling the reactive component generated by the PQ decomposition

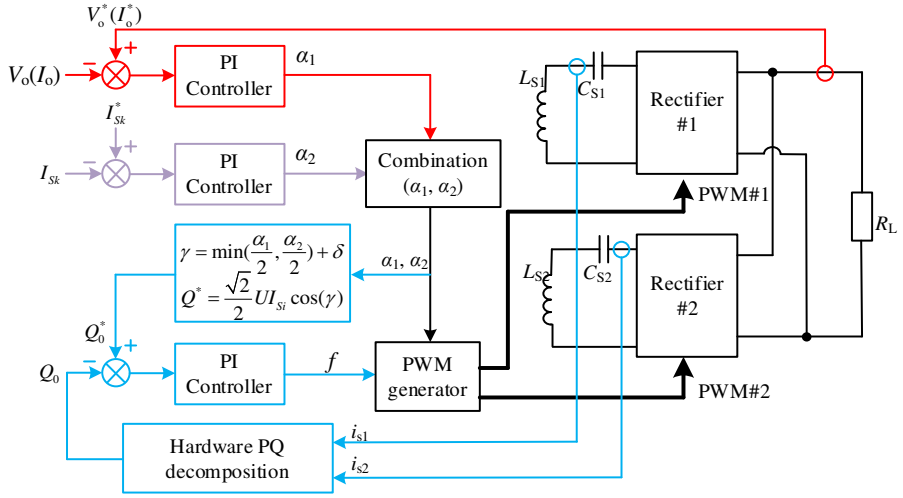

Fig. 11. Control strategy diagram of the proposed system.

method to be zero or a constant value, the active rectifiers achieve synchronization with the induced voltages and the primary side.

B. ZVS control

Because the WPT system operates at high frequency, the switching losses are a key factor to affect the efficiency. In this paper, the phase difference γ between the primary side and the secondary side is adjusted to achieve the ZVS operation of the active rectifiers. According to [29] and [30], to achieve ZVS operation in the inverter, the phase of i_P shown in Fig. 9 should lag behind v_P. On the secondary side, the current i_S should lead the voltage v_S. Therefore, φ_{inv}, φ_{rec1}, and φ_{rec2} should satisfy the following condition to ensure ZVS operation of the rectifier:

$$\begin{cases} \varphi_{inv} \geq 0 \\ \varphi_{rec1} \geq \dfrac{\pi - \alpha_1}{2} \\ \varphi_{rec2} \geq \dfrac{\pi - \alpha_2}{2} \end{cases} \tag{20}$$

To ensure the ZVS of all the switches, the phase angle γ should be as small as possible. Thus, the value of γ can be calculated by:

$$\gamma = \min\left(\frac{\alpha_1}{2}, \frac{\alpha_2}{2}\right) - \delta \tag{21}$$

where δ represents the margin to achieve ZVS and is set to be 5° in this paper.

As a result, the value of reactive power component Q_0^* for synchronization should be:

$$Q_0^* = \frac{\sqrt{2}}{2} U I_S \cos(\gamma) \tag{22}$$

When (22) is satisfied, ZVS is achieved and the phase locking is realized at the same time.

C. Three control loops

The whole control strategy diagram of the proposed dual-receiver WPT system is shown in Fig. 11. Three control goals including the current balance, constant voltage output, and ZVS is achieved by controlling α_1, α_2, and f. This control strategy is composed of three control loops. The combination of α_1 and α_2 is generated by the current balance controller and the constant voltage controller simultaneously. As analyzed in Fig. 10, both α_1 and α_2 have a monotonic effect on the current ratio. Thus, in order to avoid the situation where a certain conduction angle is quite small, a main control angle between α_1 and α_2 needs to be chosen. The main control angle is determined by the value of I_{S1} and I_{S2} during the system start-up. For example, if $I_{S1}>I_{S2}$, then α_1 is selected to be the variable in the constant-voltage control loop. Then α_2 is varied to control the current ratio to be one. After the values of α_1 and α_2 are determined by both the current balance controller and constant voltage controller, the phase angle γ can be calculated according to (21). Finally, the reference value Q_0^* for the synchronization and the ZVS condition are generated based on (22).

V. Experimental Results

A. Prototype Setup

To validate the proposed modeling method and the control strategy, an experimental WPT system based on a dual receiver coil was built as shown in Fig. 13. Two DSPs (TMS320F28335) are chosen as the controllers on the transmitter and receiver sides respectively. The MOSFETs (C2M0080120D, 80mΩ) and (IXFX420N10T, 2.6mΩ) are used for high voltage in the inverter, and low $R_{ds(on)}$ in the rectifier respectively. Two PQ decomposition circuits are used to produce the reference signal of the dual receivers. To simulate the scenario of low voltage and high current charging, the rated output voltage and current of the system are set to be 48 V and 30 A, respectively. The experimental parameters are shown in TABLE II

TABLE II
Experimental Parameters

Symb.	Val.	Symb.	Val.
V_{dc}	400V	V_{out}	48V
I_{out}	30A	R_P	776.7mΩ
L_P	597.4uH	C_P	5.86nF
R_{S1}	25.71mΩ	R_{S2}	25.78mΩ
L_{S1}	12.57uH	C_{S1}	278.9nF
L_{S2}	12.61uH	C_{S2}	278.0nF
S_1-S_4	C2M0080120D	k	0.19
S_5-S_{12}	IXFX420N10T	f	85kHz

B. Experiment Result

Fig. 14 shows the waveforms of Q_0, V_{out}, V_{S1}, and I_P before and after synchronization. When the system is not in the

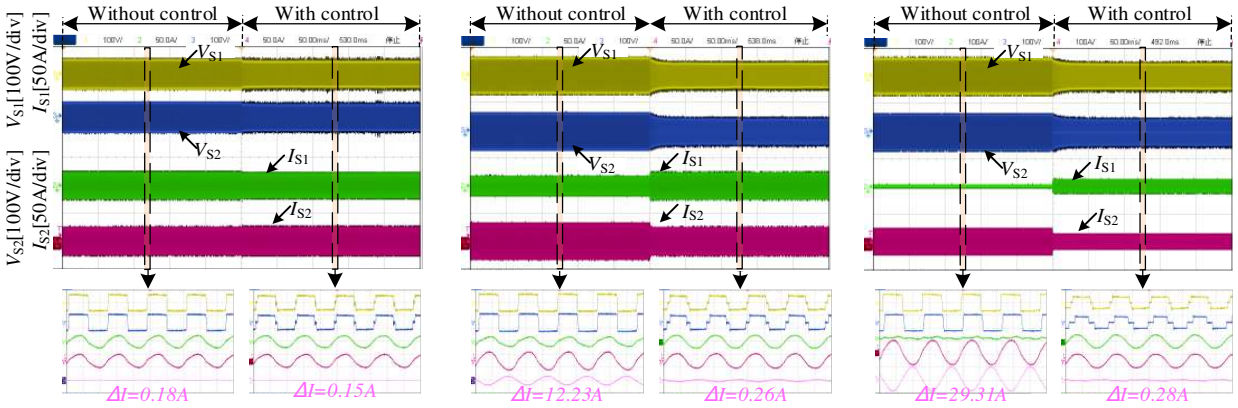

(a) Aligned (**0 mm, 0 mm, 0°**) (b) Axial offset (**30 mm, 0 mm, 0°**) (c) Plane offset (**30 mm, 0 mm, 20°**)

Fig. 12 Waveforms of currents before and after average current control

synchronized state, its output shows periodic fluctuations. When synchronized, the system has a stable output.

The AC voltage and current waveforms of the receivers under aligned, axial offset, and plane offset conditions, are shown in Fig. 12. TABLE III lists the mutual inductance parameters and the offset condition in each case. Without control, the current difference between the dual receivers is 0.32A, 12.23A, and 29.31A respectively. This verifies that the system has a large current difference even with a small mutual inductance difference. When the system is under plane offset, the current clamp happens when I_{S1} is almost zero and I_{S2} provides all the current to the load. By applying the proposed control method, the current differences are 0.16A, 0.26A, and 0.28A, respectively. It proves that the control strategy based on hardware PQ decomposition can effectively solve the current imbalance and current clamp problem. Fig. 15 shows the result of constant voltage control of the system. When the load R_L is switched from 1.6 Ω to 4.8 Ω, the system can achieve constant voltage output, and the dynamic response is 70ms.

The transient switching waveforms and driving signals of the MOSFETs S_8 and S_{12} in the two active rectifiers are shown in Fig. 16, which indicates that the ZVS is achieved in both rectifiers.

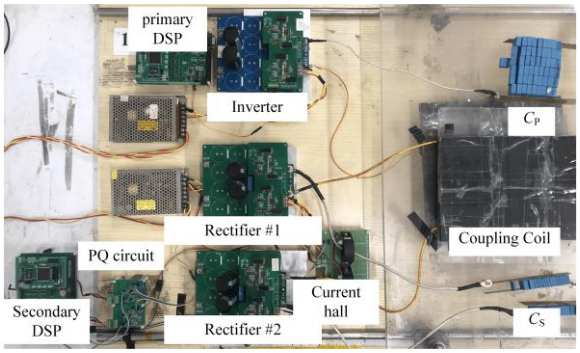

Fig. 13 Experimental setup.

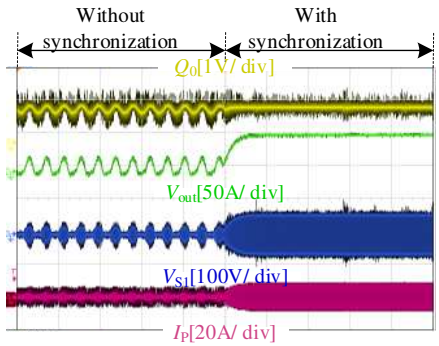

Fig. 14 Waveform of the system before and after synchronization.

TABLE III
THE VALUE OF MUTUAL INDUCTANCE IN EACH CASE

Parameters	Aligned	Axial offset	Plane offset
(X, Y, R)	(0mm, 0mm, 0°)	(30mm, 0mm, 0°)	(30mm ,0mm, 20°)
M_1	18.4uH	17.4uH	17.2uH
M_2	18.4uH	17.0uH	14.8uH

In Fig. 17, the current difference and system efficiency with and without the proposed control method is summarized and compared under three conditions. With the proposed method, the current difference can be controlled to be zero while the efficiency is always higher than that without the control. When the offset and M_k become larger, the system efficiency has more significant improvement and is close to the value under the aligned condition.

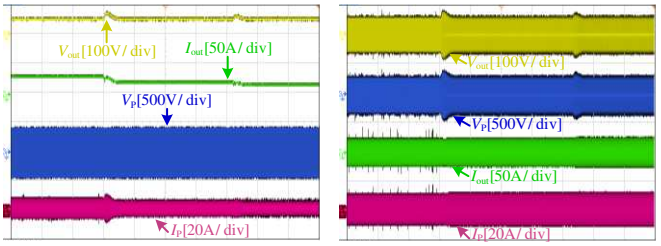

Fig. 15 Constant voltage control waveform of R_L from 1.6 Ω to 4.8 Ω.

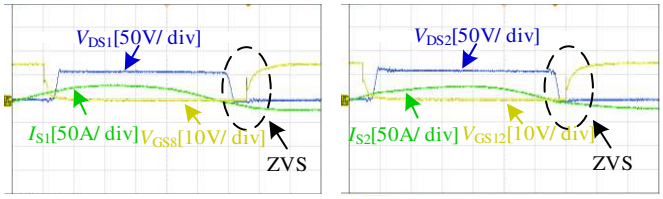

Fig. 16 ZVS waveform on the receiving side of S_8(S_{12}).

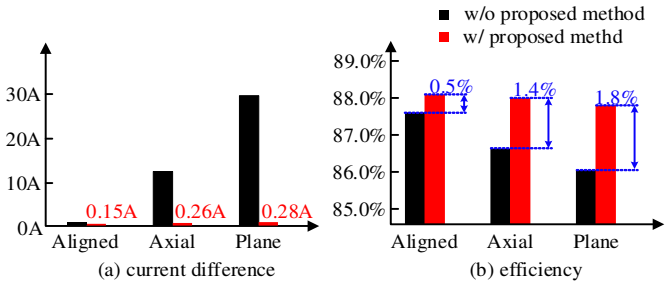

Fig. 17 Current difference and efficiency in Aligned, Axial offset, and Plane offset.

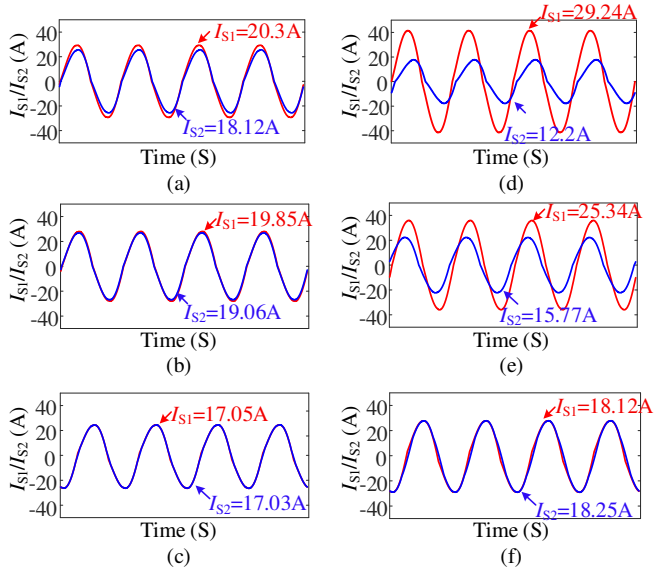

Fig. 18 Current waveforms of different current balance methods at different offsets. (a) DRT under axial offset, (b) NCL under axial offset, (c) Proposed method under axial offset. (d) DRT under plane offset, (e)NCL under plane offset, (f) Proposed method under plane offset.

C. Methods Comparison

The main methods for current balancing include adding combination of detuned resonant tank (DRT) and cross-coupling [21] and negative coupling inductance (NCL) [19] [20]. To compare with these methods, the same mutual inductance differences are used for the comparison of the current balance effect under axial offset (M_1=17.4μH M_2=17μH), and plane offset (M_1=17.2μH, M_2=14.8μH) condition. Fig. 18 shows the simulation results of these two current balance methods and the proposed method.

In Fig. 18, it can be seen that when the axial offset occurs and the mutual inductance difference is small, the maximum current difference of all methods is not above 2A. But when the mutual inductance difference becomes larger under plane offset, the current difference of the proposed method is only 0.13 A, while the current difference of the other two methods is 17.04A and 9.57A respectively. Thus, as the mutual inductance difference increases, the advantage of the proposed method is demonstrated. The comparison results are summarized in TABLE IV.

TABLE IV
COMPARISON OF CURRENT BALANCE METHODS

Reference	Year	Method	Axial offset	Plane offset	CV Output
[19]	2022	DRT	2.18A	17.04A	No
[20]	2021	NCL	0.79A	9.57A	No
This paper	-	Active rectifier	0.02A	0.13A	Yes

D. Loss Discussion

To explore the potential for more substantial efficiency enhancements, further analysis is necessary. The system loss distribution without and with the proposed current balance method is shown in Fig.19. When the mutual inductance difference is large under plane offset, the power losses of the secondary-side are decreased by 45% from 42.5W to 24.3W. The changes of the other losses are not significant after the current balance. Therefore, the reason why the system efficiency is improved is that the receivers' losses are reduced with the current balance. To further improve the efficiency, impedance matching, partial power modulation, and other methods can be investigated in the future.

VI. CONCLUSION

In this article, an accurate model for analyzing the current imbalance and current clamping of the dual-receiver WPT system is presented. The two factors M_k and λ that cause current clamping are found accordingly. Then, the QDP coil structure is used to reduce M_k under coil misalignment, and two active rectifiers are used to adjust λ, thus achieving the effect of equalizing the current. A control strategy based on hardware PQ decomposition is used to achieve current balance and constant voltage outputs. Finally, a 48V-30A dual-receiver prototype was built to validate the control strategy. The experimental results show that the current balancing and constant current output can be achieved, and the current difference between the dual receivers is decreased from 29.31A to 0.26A, while the efficiency is improved by 1.8%.

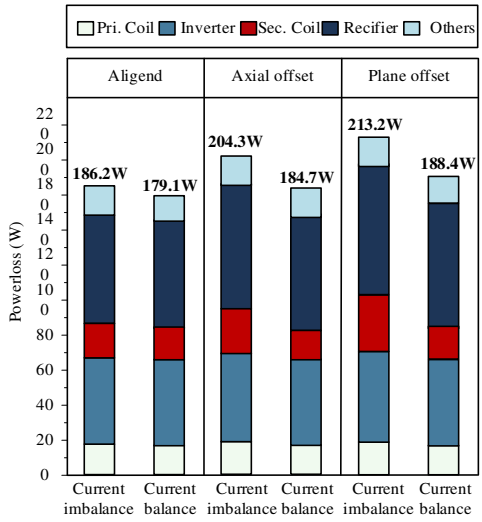

Fig. 19 The loss distribution in Aligned, Axial offset, and Plane offset.

REFERENCES

[1] D. Patil, M. K. McDonough, J. M. Miller, B. Fahimi and P. T. Balsara, "Wireless Power Transfer for Vehicular Applications: Overview and Challenges," *IEEE Trans. Transport. Electrific.*, vol. 4, no. 1, pp. 3-37, March 2018.

[2] Y. Li, T. Lin, R. Mai, L. Huang, and Z. He, "Compact double-sided decoupled coils-based WPT systems for high-power applications: Analysis, design, and experimental verification," *IEEE Trans. Transport. Electrific.*, vol. 4, no. 1, pp. 64–75, Mar. 2018.

[3] S. -J. Huang, T. -S. Lee, W. -H. Li and R. -Y. Chen, "Modular On-Road AGV Wireless Charging Systems Via Interoperable Power Adjustment," *IEEE Trans. Ind. Electron.*, vol. 66, no. 8, pp. 5918-5928, Aug. 2019.

[4] J. Wang, R. Chen, C. Cai, J. Zhang, and C. Wang, "An Onboard Magnetic Integration-Based WPT System for UAV Misalignment-Tolerant Charging With Constant Current Output," *IEEE Trans. Transport. Electrific.*, vol. 9, no. 1, pp. 1973-1984, March 2023.

[5] F. Lu *et al.*, "A Low-Voltage and High-Current Inductive Power Transfer System With Low Harmonics for Automatic Guided Vehicles," *IEEE Trans. Veh. Technol.*, vol. 68, no. 4, pp. 3351-3360, Apr. 2019.

[6] C. Zhu *et al.*, "Analysis and Design of Cost-Effective WPT Systems With Dual Independently Regulatable Outputs for Automatic Guided Vehicles," *IEEE Trans. Power Electron.*, vol. 36, no. 6, pp. 6183-6187, Jun. 2022.

[7] C. Jiang, K. T. Chau, C. Liu, C. H. T. Lee, W. Han, and W. Liu, "Move-and-Charge System for Automatic Guided Vehicles," *IEEE Trans. Magn.*, vol. 54, no. 11, pp. 1-5, Nov. 2018.

[8] Y. Wang *et al.*, "Research on 11kW Wireless Charging System for Electric Vehicle Based on LCC-SP Topology and Current Doubler," *2020 IEEE Energy Conversion Congress and Exposition (ECCE)*, 2020, pp. 820-827.

[9] K. Huang, H. Hsieh, and R. Wai, "Phase-shifted full-bridge converter for a half-current-multiplier rectifier using an autotransformer-based filter," *IEEE Trans. Transp. Electrific.*, vol. 6, no. 1, pp. 199–212, Mar. 2020.

[10] J. Y. Shin, H.-W. Kim, K.-Y. Cho, S.-S. Hwang, S.-K. Chung, and G.-B. Chung, "Analysis of LLC resonant converter with current-doubler rectification circuit," *in Proc. 16th Int. Power Electron. Motion Control Conf. Expo.*, 2014, pp. 162–167.

[11] L. Shi, A. Delgado, R. Ramos, and P. Alou, "A Wireless Power Transfer System With Inverse Coupled Current Doubler Rectifier for High-Output Current Applications," *IEEE Trans. Ind. Electron.*, vol. 69, no. 5, pp. 4607-4616, May 2022.

[12] X. Xie, C. Xie, J. Wang, Y. Li, Y. Du, and L. Li, "Constant Current Output Control Based on Cross-Coupling Compensation in Multireceiver WPT System Using Active Rectifier," *IEEE Trans. Transport. Electrific.*, vol. 9, no. 1, pp. 1960-1972, March 2023.

[13] H. Yuan, C. Wang, and D. Xia, "Research on Input-Parallel Single-Switch WPT System With Load-Independent Constant Voltage Output," *IEEE Trans. Transport. Electrific.*, vol. 9, no. 1, pp. 1888-1896, March 2023.

[14] Y. Li *et al*., "Efficiency Analysis and Optimization Control for Input-Parallel Output-Series Wireless Power Transfer Systems," *IEEE Trans. Power Electron.*, vol. 35, no. 1, pp. 1074-1085, Jan. 2020.
[15] S. Y. Choi *et al*, "Generalized Models on Self-Decoupled Dual Pick-up Coils for Large Lateral Tolerance," *IEEE Trans. Power Electron*, vol. 30, no. 11, pp. 6434-6445, Nov. 2015
[16] R. Mai, Y. Luo, B. Yang, Y. Song, S. Liu, and Z. He, "Decoupling Circuit for Automated Guided Vehicles IPT Charging Systems With Dual Receivers," *IEEE Trans. Power Electron.*, vol. 35, no. 7, pp. 6652-6657, Jul. 2022.
[17] X. Xie, C. Xie, and L. Li, "Wireless Power Transfer to Multiple Loads Over a Long Distance With Load-Independent Constant-Current or Constant-Voltage Output," *IEEE Trans. Transport. Electrific.*, vol. 6, no. 3, pp. 935-947, Sept. 2020.
[18] G. Ke *et al*., "Research on IPT resonant converters with high misalignment tolerance using multicoil receiver set," *IEEE Trans. Power Electron*., vol. 35, no. 4, pp. 3697-3712, Apr 2020.
[19] H. Polat *et al*., "Balancing of common DC-Bus parallel-connected modular inductive power transfer systems," *IEEE J. Emerg. Sel. Topics Power Electron*., vol. 10, no. 2, pp. 1587-1596, Apr 2022.
[20] M. Yamaguchi, K. Kusaka and J. -i. Itoh, "Current Balancing Method in Parallel Connected Inverter Circuit for Megahertz WPT System," *2021 IEEE 30th Inter. Symposium on Ind. Electron.*, 2021, pp. 1-6.
[21] M. Luo, Z. Huang, B. Zou, and Z. Huang, "Current Balance Design for Inductive Power Transfer Systems with Secondary Multiple Parallel Branches," *IECON 2022 48th Annual Conference of the IEEE Ind. Electronics Society*, 2022, pp. 1-5.
[22] Zaheer, D. Kacprzak and G. A. Covic, "A Bipolar Receiver Pad in A Lumped IPT System for Electric Vehicle Charging Applications," 2012 IEEE Energy Conversion Congress and Exposition (ECCE), 2012, pp. 283-290.
[23] Y. Li et al., "Efficiency Analysis and Optimization Control for Input-Parallel Output-Series Wireless Power Transfer Systems," IEEE Trans. on Power Electron., vol. 35, no. 1, pp. 1074-1085, Jan. 2020.
[24] K. Zhao, G. Ning, R. He, H. Yang, H. Wang, and M. Fu, "An Unsymmetrical Driving Scheme for Inductive Power Transfer Systems Using Decoupled Transmitter Coils," IEEE Journal of Emerging and Selected Topics in Ind. Electron., vol. 4, no. 2, pp. 614-624, Apr. 2023.
[25] Y. Chen et al., "A Hybrid Inductive Power Transfer System with Misalignment Tolerance Using Quadruple-D Quadrature Pads," IEEE Trans. on Power Electron., vol. 35, no. 6, pp. 6039-6049, Jun. 2020.
[26] Y. Li, R. Mai, L. Lu, and Z. He, "Active and Reactive Currents Decomposition-Based Control of Angle and Magnitude of Current for a Parallel Multiinverter IPT System," *IEEE Trans. Power Electron*., vol. 32, no. 2, pp. 1602-1614, Feb. 2017.
[27] Y. Tang *et al*, "A New Controller for Bidirectional Wireless Power Transfer Systems," *IEEE Trans. Power Electron*., vol. 33, no. 10, pp. 9076-9087, Oct. 2018.
[28] S. Zhao, Y. Li, D. Wu, and R. Mai, "Current-Decomposition-Based Digital Phase Synchronization Method for BWPT System," *IEEE Trans. Power Electron*., vol. 36, no. 11, pp. 12183-12188, Nov. 2021.
[29] X. Zhang et al., "A Control Strategy for Efficiency Optimization and Wide ZVS Operation Range in Bidirectional Inductive Power Transfer System," IEEE Trans. Ind. Electron., vol. 66, no. 8, pp. 5958–5969, Aug. 2019.
[30] Y. Li, W. Sun, X. Zhu and J. Hu, "A Hybrid Modulation Control for Wireless Power Transfer Systems to Improve Efficiency Under Light-Load Conditions," *IEEE Trans. Power Electron*. vol. 69, no. 7, pp. 6870-6880, Jul. 2022.

Yong Li (S'15-M'19-SM'21) received the B.Sc. and Ph.D. degrees from the School of Electrical Engineering, Southwest Jiaotong University, Chengdu, China, in 2013 and 2017, respectively. From 2017 to 2018, he was a Research Associate at the Department of Electrical Engineering, The Hong Kong Polytechnic University, and subsequently, he was a Post-Doctoral Fellow with the same department. He is currently an Associate Professor with Southwest Jiaotong University, Chengdu, China. His main research interests are wireless power transfer and energy harvesting.

Junwen Chen received the B.S. degree in electrical engineering and automation from the School of Electrical Engineering, Southwest Jiaotong University, Chengdu, China, in 2020, where he is currently working toward the Master degree. His main research interest focuses on wireless power transfer.

Yeran Liu (S'17-M'20) received B.Sc. and Ph.D. degrees in electrical engineering from Southwest Jiaotong University, Chengdu, China, in 2015 and 2020, respectively, where he is currently working as an assistant professor. From 2018-2019, he was a visiting Ph.D. student at the Department of Electrical and Computer Engineering, The University of Auckland, Auckland, New Zealand. His research interests include modeling and optimal control for wireless power transfer systems.

Xing Zhao (Member, IEEE) received the B.Eng. degree from Nanjing University of Aeronautics and Astronautics, Nanjing, China, in 2014, and the Ph.D. degree from The Hong Kong Poly-technic University, Hong Kong SAR, in 2020, both in Electrical Engineering. He is currently a Lecturer in the School of Physics, Engineering and Technology with University of York, UK. His research interests include advanced electri-cal machines and power electronics for electric vehicles and renewable energy systems.

Minfan Fu (Senior Member, IEEE) received the B.S., M.S., and Ph.D. degrees in electrical and computer engineering from the University of Michigan Shanghai Jiao Tong University Joint Institute, Shanghai Jiao Tong University, Shanghai, China, in 2010, 2013, and 2016, respectively. From 2016 to 2018, he held a Postdoctoral position with the Center for Power Electronics Systems (CPES), Virginia Polytechnic Institute and State University, Blacksburg, VA, USA. He is currently an Assistant Professor with the School of Information Science and Technology, ShanghaiTech University, Shanghai, China. He holds one U.S. patent, seven Chinese patents, and has authored or coauthored more than 80 papers in prestigious IEEE journals and conferences. His research interests include megahertz wireless power transfer, high-frequency power conversion, high-frequency magnetic design, and application of wide-bandgap devices

Zhengyou He (Senior Member, IEEE) received the B.Sc. degree and M. Sc. degree in Computational Mechanics from Chongqing University, Chongqing, China, in 1992 and 1995, respectively. He received the Ph.D. degree in the School of Electrical Engineering from Southwest Jiaotong University, Chengdu, China, in 2001. Currently, he is a Professor in the School of Electrical Engineering at Southwest Jiaotong University. His research interests include signal process and information theory applied to electrical power system, and application of wavelet transforms in power system.